Monolithic bifocal zone-plate lenses for confocal collimation of laser diodes

Tong Jiang,[1] Qi-Dai Chen,[1,4] Jun Zhang,[2] Zhen-Nan Tian,[3] Li-Gang Niu,[1] Qi-Song Li,[3] Hai-Yu Wang,[1] Li Qin,[2] and Hong-Bo Sun[1,3,5]

[1]*State Key Laboratory on Integrated Optoelectronics, College of Electronic Science and Engineering, Jilin University, 699 Qianjin Street, Changchun 130012, China*

[2]*Changchun Institute of Optics, Fine Mechanics and Physics, Chinese Academy of Sciences, Changchun 130033, China*

[3]*College of Physics, Jilin University, 199 Jiefang Road, Changchun 130023, China*

[4]*e-mail: chenqd@jlu.edu.cn*

[5]*e-mail: hbsun@jlu.edu.cn*

Received May 6, 2013; revised August 24, 2013; accepted August 24, 2013; posted August 26, 2013 (Doc. ID 190056); published September 17, 2013

An elliptical monolithic bifocal zone plate as a collimating lens, whose two focal lengths in the orthogonal directions match the different beam waist positions of the fast and slow axes' light from edge-emitting laser diodes, is proposed and experimentally demonstrated by employing femtosecond laser direct writing technology. The high-quality eight-level zone plate exhibits a diffraction efficiency of 92.9%, which is much higher than those ever reported. Shaped by the elliptical lens, the laser diodes' divergence angles are simultaneously reduced from 65° (1134 mrad, fast axis) and 24° (418 mrad, slow axis) to 7.7 and 136.5 mrad, respectively.

OCIS codes: (230.3990) Micro-optical devices; (120.4610) Optical fabrication.
http://dx.doi.org/10.1364/OL.38.003739

Due to the narrow slit shape of the end facet of an edge-emitting laser diode (EELD) arising from the extremely thin active layer consisting generally of quantum well structures, the output laser beam is divergent with greatly different angles along the directions perpendicular (fast axis) and parallel (slow axis) to the slit and expands with rapidly varying elliptical cross sections. Optical beam transformation systems are therefore needed for most laser diode applications such as laser communication, optical storage, optical gyro, laser printing, and laser micronanofabrication [1–3]. The inconsistency of laser beam divergence angles along different axes makes it difficult to achieve confocal collimation with a single device. Lloyd's mirror interference [4], two-plane parallel mirrors [5], stripe mirror, and *V*-stack mirror [6,7] have been used to reshape the output beam. However, most of them used pairs or combinations of aspheric lenses or cylindrical mirrors [8–10]. The beam collimating systems are thus bulky and difficult to align and maintain. Compared to refractive bulk elements, diffractive optical elements are characterized by being much thinner, easy to fabricate, and flexible to design, so it has been widely used as a substitute for the common refractive bulky lens for the reduction of device volume, weight, and cost. Yet the difficulty in micro-optical alignment and long-term stability of the combined pair system are still problematic for practical use.

In this Letter, we demonstrate a monolithic eight-level elliptical zone-plate lens that features double focus of different focal lengths along the long and the short axes, which cope with the different positions of the beam waists of the EELDs along the fast and slow axes. The plates are theoretically designed and experimentally created with femtosecond laser direct writing (FsLDW). Diffraction efficiency up to 92.9% is achieved. The technology allows for customized zone-plate lens design depending on the individual output of the laser diodes. Here, the double focus does not mean there is multiorder diffraction along the optical axis of a wave zone plate, but they result from the two different axis lengths of the elliptical plate shape. Both foci are from the first-order diffraction (main focus) whose efficiency is much higher than the high-order ones.

The theoretical design of the monolithic bifocal zone plate as the collimating lens of the laser diodes is shown in Fig. 1(a). We set d as the work distance between the collimating lens and the laser diode. With the known parameters of the EELD, such as the sizes of the emitting window and divergence angles, $R_{s\min}$ (the minimum radius of the beam along the slow axis) and $R_{f\min}$ (the minimum radius of the beam along the fast axis) are calculated based on the simple trigonometric relation as shown in Figs. 1(b) and 1(c).

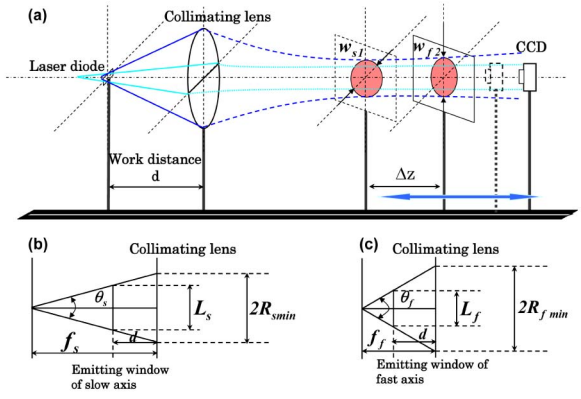

Fig. 1. (a) Theoretical design of the collimating zone-plate lens and divergence angle testing setup. (b) and (c) The schematic diagrams of the focal length and radius calculation.

The $R_{s\min}$ and $R_{f\min}$ are calculated according to

$$R_{s\min} = f_s \cdot \tan\left(\frac{\theta_s}{2}\right) = \left(\frac{L_s}{2\tan\left(\frac{\theta_s}{2}\right)} + d\right)\tan\left(\frac{\theta_s}{2}\right), \quad (1)$$

$$R_{f\min} = f_f \cdot \tan\left(\frac{\theta_f}{2}\right) = \left(\frac{L_f}{2\tan\left(\frac{\theta_f}{2}\right)} + d\right)\tan\left(\frac{\theta_f}{2}\right), \quad (2)$$

where L_s and L_f are the sizes of the emitting windows, θ_s and θ_f are the divergence angles, and f_s and f_f are the focal lengths of the slow and the fast axes, respectively.

The multilevel zone-plate lens takes the form of a Fresnel zone plate, where the radius of the nth phase shift circle (the outer radius of the nth zone) is determined according to a simple trigonometric relation by the following equation:

$$r_n = \sqrt{\left(f + \frac{n\lambda}{2}\right)^2 - f^2}, \quad (3)$$

where λ is the wavelength of the incident light through the zone plate and f is the distance from the center of the zone plate to the focus. The initial zone plate is an amplitude type, which means that the zones alternate between opaque and transparent ones. However, it has low diffraction efficiency since half of the incident light is wasted, as it is blocked by the opaque zones. In order to make full use of the incident light, phase-type zone plates are developed, where opaque zones are replaced by phase-retarding zones that retard the light passing through them to make it identical in phase to that passing through the nonretardation zones so as to cause constructive interference at the foci. To further improve the diffraction efficiency, a phase-type zone plate is made into a multilevel one, where each zone is divided into L subzones, each of which are short by $2\pi/L$ in phase retardation compared with their inner neighbors. The level of the zones helps weaken the high-order diffraction to concentrate more light into the main focuses. The radius of the mth phase shift circle is written as

$$r_m = \sqrt{\left(f + \frac{m\lambda}{L}\right)^2 - f^2}, \quad (4)$$

where m is the sequence number of the mth subzone, f is the focal length, and λ is the wavelength of the incident light. When m is large enough and $(m\lambda/L)^2 \ll (2\ m\lambda f)/L$, Eq. (4) is reduced to Eq. (5):

$$r_m \approx \sqrt{\frac{2\ m\lambda f}{L}}. \quad (5)$$

The f is expressed as

$$f = \frac{r_m^2 L}{2\ m\lambda} = \frac{r_M^2 L}{2M\lambda} = \frac{R^2 L}{2M\lambda} = \frac{R^2}{2N\lambda}, \quad (6)$$

where R is the radius of the multilevel zone-plate lens, N is the number of zones, and M is the total number of subzones with $M = NL$. Equation (6) indicates that the focal length is independent of the number of levels, so we adjust L to improve the diffraction efficiency without causing concomitant change on the focal length. With the calculation of f_s and f_f, $R_{s\min}$ and $R_{f\min}$ in Eqs. (1) and (2), N is derived from Eq. (6). With $M = NL$, we attain the total number of subzones. To satisfy M along the slow and the fast axes, a greater M is chosen. With M specified, the minimum radii of the slow and the fast axes are calculated by Eq. (6). As M increases, the radius also increases with the focal length unchanged so that the collimating lens covers the all-emitting laser pass through it along both axes. In addition, the diffraction efficiency of the multilevel zone-plate lens is calculated by

$$\eta = \mathrm{sinc}^2(1/L) = \left[\frac{\sin(\pi/L)}{\pi/L}\right]^2. \quad (7)$$

For $L = 2$, $L = 4$, and $L = 8$, the theoretical efficiencies are 40.5%, 81.0%, and 95.1%, respectively.

We use a FsLDW for the zone-plate fabrication [11,12]. As a direct writing technology, FsLDW is a mask-free technology with high accuracy and capabilities of prototyping structures with arbitrary shape. Combined with the flexibility of a diffractive optics design, the technology facilitates greatly the manufacture of customized collimating lenses for individual semiconductor lasers with different parameters.

Experimentally, the zone plates are made of commercial photoresin SU-8 with a refractive index of 1.593 at 808 nm. The femtosecond laser pulses are tightly focused by a 100× objective with a numerical aperture of 1.40 to induce polymerization in the focal spot [13]. With the zone-plate lens data file created by computer and controlled by the fabrication program, a 3D air-bearing stage (Aerotech Inc.) moves three dimensionally relative to the sample resist. When the scanning is finished, the slide is laid on the hotplate again for 1 min at 65°C and 10 min at 95°C, namely, postbake, which helps the exposed SU-8 molecules thoroughly cross-link. After this treatment and having cooled down, the slide is immersed in the developer for SU-8, which dissolves the uncross-exposed resin and thus reveals the zone-plate lens.

The eight-level elliptical zone plates have two different foci along two orthogonal directions. We study the intensity distribution and dispersion properties of the eight-level elliptical zone plates. Shown in Figs. 2(a) and 2(b) are the scanning electron microscopic (SEM) images of the elliptical zone plates with $r_1 = 300$ μm and $r_2 = 150$ μm along the long and the short axes, respectively. The magnified SEM image Fig. 2(b) clearly shows that it is the eight-level structure. The surface roughness of the zone-plate lens, although not measured directly here due to technical difficulties, is believed to be at the same level of several nanometers as those achieved by us previously and by others [14,15]. The shrinkage rate of approximately 1% of the SU-8 is considered and precompensated. Based on the Huygens–Fresnel principle, the theoretical distributions of this elliptical zone plate are simulated in Figs. 2(c) and 2(d). Experimentally, we

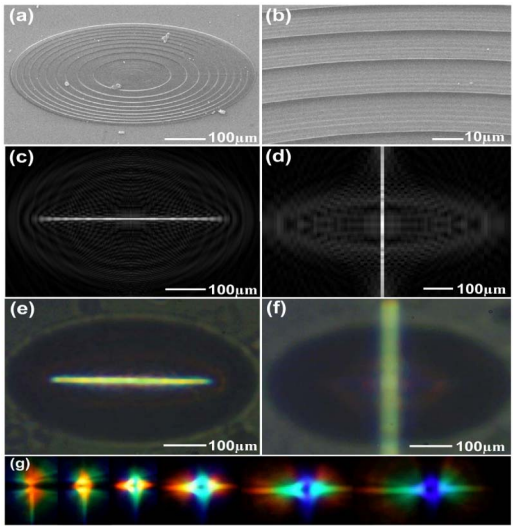

Fig. 2. Multilevel zone-plate lenses that were fabricated by FsLDW. (a) Front-view SEM image. (b) Partially enlarged view image. (c) and (d) The theoretical intensity distributions of the fast and the slow axes. (e) and (f) The experimentally measured intensity distribution observed through the microscope with a 4× objective lens. (g) Color dispersion in planes perpendicular to the optical axis.

obtain both of the corresponding focal spots at 3.388 and 15.246 mm. Figures 2(e) and 2(f) agree well with the theoretical results. It is well known that the diffractive elements exhibit negative dispersion. The intrinsic negative dispersion performance of diffractive elements, if combined with refractive optical elements, may lead to ideal zero-dispersion imaging devices. Similarly, the asymmetric zone plate also has negative dispersion. The color images are discerned in a plane perpendicular to the optical axis under illumination of white light from a halogen lamp. Different colors show up in turn as the probe moves through the focal planes of different wavelengths, as shown in Fig. 2(g), and the same colors along the fast and the slow axes do not appear at the same planes, as the zone-plate lens possesses different focal lengths along the two axes. Experimentally, the red color in the short axis is observed as the corresponding focal spots at 7 and 1.8 mm; the yellow color appears at 7.7 and 1.94 mm; the green color appears at 8.1 and 2 mm, the blue color at 9.1 and 2.2 mm, and the purple color at 9.9 and 2.45 mm.

The confocal collimation capabilities of the monolithic lenses are tested. An EELD of 808 nm wavelength is selected, which is measured to possess a divergence angle of 65° and 24° along the fast and slow axes, respectively, and an emitting size of 1.5 and 10 μm along fast and slow axes, respectively (provided by the Changchun Institute of Optics, Fine Mechanics and Physics, Chinese Academy of Sciences). For a compact combination of the laser and collimating zone plates, we set the back work distance to 400 μm. The focal lengths and radii of the fast and slow axes are obtained according to Eqs. (1) and (2), that is, $f_f = 401$ μm, $f_s = 423$ μm, $R_f = 233$ μm, and $R_s = 89$ μm. According to Eq. (6), N has different values of 11.58 and 84.6. To satisfy M along the slow and the fast axes, a larger M is chosen. The total number of subzones $M = NL = 84 \times 8 = 674$. Then, R_s is recalculated as 240 μm from Eq. (6). The radii and heights of all subzones are thus specified, and then the model of the zone-plate lens is created and used for the fabrication of the elliptical zone plates with two foci.

Shown in Figs. 3(a) and 3(b) are top-view SEM images and magnified SEM images of the collimating zone plate prepared by FsLDW. The diffraction efficiency of the collimating zone plates is measured by a homemade optical characterization setup shown in Fig. 3(c). First, we set all the elements on the slideway and align their centers; then we eliminate the influence of ambient light. The attenuator is used to adjust the intensity of the laser to avoid the oversaturation of the detector. The laser beam is focused by the zone plate and magnified by the objective lens. With an iris to circumscribe the incident light, we can ensure that only the laser that is focused by the zone plate is received by the detector. First, the voltage v_1 on the oscilloscope is recorded. Then, we remove the zone plate without changing the aperture of the iris and an equivalent thickness SU-8 film is placed into the beam since the reflection losses in SU-8 will be taken into account. We then record the voltage v_2 on the oscilloscope. The diffraction efficiency is calculated by $\eta = v_1/v_2$. We test several zone plates with the same parameters, and each diffraction efficiency is determined to be no lower than 90%. The best diffraction efficiency reaches 92.9%, close to the theoretical value of 95.1%. The difference is mainly attributed to the fabrication error along with shrinkage and dilation of the material.

The divergence angle of a Gaussian beam is defined as

$$\theta_0 = \lim_{z\to\infty} \frac{w(z)}{z} = \frac{\lambda}{\pi w_0}, \tag{8}$$

where z is the distance away from the beam waist, $w(z)$ is the diameter of the beam (defined as the diameter, where the field intensity drops to $1/e^2$ of their axial values) at z, and w_0 is the diameter of the beam waist. This equation provides two ways of measuring the divergence angle: one is to calculate the divergence angle with the diameter of the beam waist w_0; the other way is to calculate the divergence angle with two or more diameters at different positions after the collimating lens and the distance in between, i.e.,

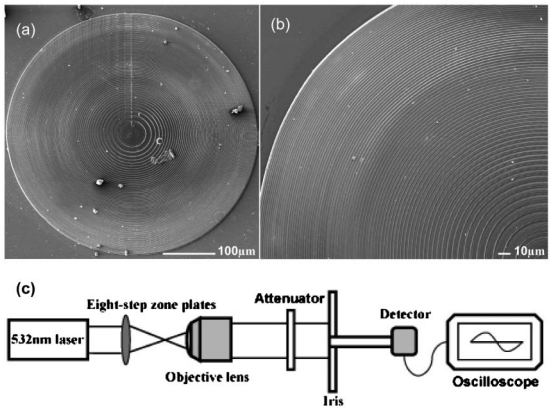

Fig. 3. Collimating zone-plate lens fabricated by FsLDW. (a) Top-view SEM image. (b) Magnified SEM image. (c) The schematic image of the optical characterization setup.

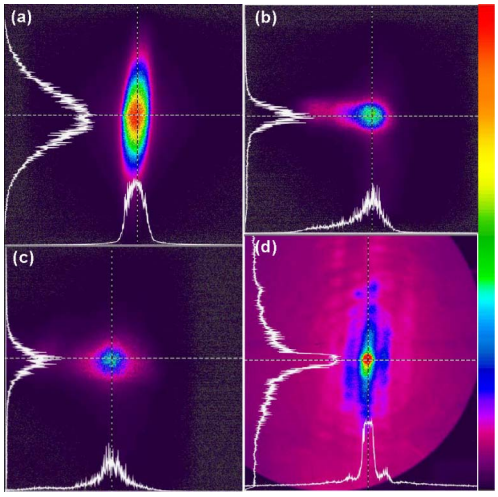

Fig. 4. Laser beam shaping by zone plates. (a) The laser spot without any collimating lens. (b) and (c) The collimated laser spots from an eight-level elliptical zone plate at two positions with an interval of 100 mm. (d) The collimated laser spots with circular eight-level Fresnel zone plate.

$$\theta_0 \approx \frac{w_1(z_1) - w_2(z_2)}{z_1 - z_2} = \frac{w_1 - w_2}{\Delta z}. \tag{9}$$

The second approach should be adopted when the position of the beam waist is unknown; thus, we do not have to know the absolute value of z. To measure the diameter of the beam at a certain position, we employ the commercial software BeamGage (Ophir-Spiricon Inc.) to analyze the laser spot based on the second moment principle, which autotunes and selects the best collimating results. Figure 4(a) shows the laser spot without any collimating lens. Obviously, the shape is elliptical. However, after the elliptical zone plates, the spot almost changes into a round one. Shown in Figs. 4(b) and 4(c) are the results of the analysis of the laser spots with collimating results at two different positions with an interval of 100 mm. The measured diameters of the fast axis are 13.59 and 14.36 mm, respectively. The measured diameters of the slow axis are 41.12 and 54.77 mm, respectively. The divergence angles according to Eq. (9) are 7.7 and 136.5 mrads for the fast and slow axes, respectively. For comparison, a circular zone-plate lens is prepared and used for the laser shaping. Figure 4(d) shows the laser spot collimated by a single-focus circular eight-level Fresnel zone plate with $r = 1$ mm, but there is no apparent collimating effect. Therefore, the designed collimating multilevel zone plate can significantly reduce the divergence angle along the fast and slow axes. Because of the negligible optical absorption of SU-8 at 808 nm, no output degrading due to thermal effect is observed in any of the measurements. This remains true for other typical laser diodes' output wavelengths of 980 nm and 1.55 μm.

In summary, we present a monolithic bifocal eight-level zone-plate lens for the collimation of an edge-emitting semiconductor laser, which exhibits a fine beam-shaping performance compared with the single-focus circular structure. Its efficiency reaches as high as 92.9%, comparable to the theoretical value of 95.1%. The lens reduces the divergence angles of an EELD from 65° and 24° along the fast and slow axes, respectively, to 7.7 and 136.5 mrads, respectively. Not only is the device's performance high, it should be pointed out that the device is small, lightweight, and customized according to the individual requirements of laser diodes, and they are alignment free and maintenance free, which is particularly suitable for compact leave-alone micro-optical systems.

The authors acknowledge the financial support from the National Natural Science Foundation of China (NSFC) under Grant Nos. 90923037, 61137001, 61127010, and 61008035.

References

1. F. M. Dickey, Opt. Photon. News **14**(4), 30 (2003).
2. E. Murphy, Nat. Photonics **4**, 287 (2010).
3. D. Wu, L.-G. Niu, Q.-D. Chen, R. Wang, and H.-B. Sun, Opt. Lett. **33**, 2913 (2008).
4. T. Fukushima, K. Sakaguchi, and Y. Tokuda, Opt. Rev. **18**, 287 (2011).
5. W. A. Clarkson and D. C. Hanna, Opt. Lett. **21**, 375 (1996).
6. P. Modh, J. Backlund, N. Eriksson, J. Bengtsson, S. Kristjansson, and A. Larsson, Opt. Lett. **27**, 574 (2002).
7. D. Beckmann, D. Schnitzler, D. Schaefer, J. Gottmann, and I. Kelbassa, Opt. Express **19**, 25418 (2011).
8. J. A. Hoffnagle and C. M. Jefferson, Opt. Eng. **42**, 3090 (2003).
9. L. Vaissie, W. Mohammed, and E. G. Johnson, Opt. Lett. **28**, 651 (2003).
10. M. Serkan and H. Kirkici, IEEE Sens. J. **9**, 36 (2009).
11. K. S. Lee, R. H. Kim, D. Y. Yang, and S. H. Park, Prog. Polym. Sci. **33**, 631 (2008).
12. R. Buividas, M. Mikutis, T. Kudrius, A. Greicius, G. Slekys, and S. Juodkazis, Lith. J. Phys. **52**, 301 (2012).
13. W. Xiong, Y. S. Zhou, X. N. He, Y. Gao, M. Mahjouri-Samani, L. Jiang, T. Baldacchini, and Y. F. Lu, Light Sci. Appl. **1**, e6 (2012).
14. D. Wu, S.-Z. Wu, L.-G. Niu, Q.-D. Chen, R. Wang, J.-F. Song, H.-H. Fang, and H.-B. Sun, Appl. Phys. Lett. **97**, 031109 (2010).
15. E. Brasselet, M. Malinauskas, A. Zukauskas, and S. Juodkazis, Appl. Phys. Lett. **97**, 211108 (2010).